UNIVERSITY OF BATH

University of Bath

Bean seedling growth enhancement using magnetite nanoparticles

Nádia M. Duran[a], Maria Medina-Llamas[b], João G. B. Cassanji[a], Rafael G. de Lima[a], Eduardo de Almeida[a], Willian R. Macedo[c], Davide Mattia[b] and Hudson W. Pereira de Carvalho[a,*]

[a]Laboratory of Nuclear Instrumentation (LIN), Center for Nuclear Energy in Agriculture (CENA), University of São Paulo (USP), Piracicaba, SP, 13416000, Brazil.

[b]Department of Chemical Engineering, University of Bath, BA2 7AY Bath, United Kingdom.

[c]Crop Physiology and Metabolism Lab, Institute of Agricultural Science, Federal University of Viçosa, Campus Rio Paranaíba, Rio Paranaíba, MG, 38810000, Brazil.

*Corresponding author:

Email: hudson@cena.usp.br

Phone: + 55 19 3429 4737

1 **ABSTRACT**

2 Advanced fertilizers are one of the top requirements to address rising global food demand. This

3 study investigates the effect of bare and polyethylene glycol-coated Fe_3O_4 nanoparticles on the

4 germination and seedling development of *Phaseolus vulgaris* L. Although the germination rate

5 was not affected by the treatments (1 to 1 000 mg Fe L^{-1}), seed soaking in Fe_3O_4-PEG at 1 000

6 mg Fe L^{-1} increased radicle elongation (8.1 ± 1.1 cm vs. 5.9 ± 1.0 cm for the control).

7 Conversely, $Fe^{2+}/Fe^{3+}_{(aq)}$ and bare Fe_3O_4 at 1 000 mg Fe L^{-1} prevented the growth. X-ray

8 spectroscopy and tomography showed that Fe penetrated in the seed. Enzymatic assays showed

9 that Fe_3O_4-PEG was least harmful treatment to α-amylase. The growth promoted by the Fe_3O_4-

10 PEG might be related to water uptake enhancement induced by the PEG coating. These results

11 show the potential of using coated iron nanoparticles to enhance the growth of common food

12 crops.

13 **KEYWORDS:** *Phaseolus vulgaris* L., Fe_3O_4 nanoparticle, polyethylene glycol, germination,

14 X-ray spectroscopy

15

16

INTRODUCTION

Due to the increase in human population, the agriculture is under pressure to intensify the use of chemical fertilizers to meet food demand. And yet, a large portion of fertilizers directly applied to the soil is lost by water leaching, irreversible/strong adsorption or, in the case of nitrogen sources, by evaporation. This loss negatively affects the environment, the sustainability of the sources of mineral inputs and the economic performance of agricultural activity. In this context, using nano-sized fertilizers could significantly increase uptake by plants, paving the way to a more sustainable strategy to improve nutrient delivery.[1]

Although Fe is the second most abundant metal in the earth's crust,[2] it is mostly found as Fe^{3+} oxides and oxyhydroxides in cultivated (aerated) soils, which are insoluble (goethite, ferrihydrite and hematite with K_{sp} values ranging from 10^{-37} to 10^{-44}).[3] This means that even though the total Fe content is high, its availability to plants is still low. Iron uptake can be divided in two categories: Strategy I for nongraminaceous plants and Strategy II for graminaceous. Nongraminaceous species take up Fe by three reactions: (i) excreting protons from the roots to the rhizosphere, reducing the soil solution pH and thus increasing Fe^{3+} solubility; (ii) reducing Fe^{3+} to Fe^{2+} by Fe^{3+}-chelate reductase; (iii) plasmalemma transport of Fe^{2+} by iron transporters. Roots of graminaceous species release phytosiderophores that chelate Fe^{3+} in the rhizosphere, and then specific plasmalemma transporters take the Fe^{3+}-phytosiderophores complexes.[4]

In plants, Fe plays an important role in the photosynthetic activity, biosynthesis of many enzymes, Fe-S protein clusters and heme proteins like cytochromes, is required for chloroplast thylakoids structure and maintenance, and chlorophyll synthesis.[2]

Iron oxide nanoparticles are currently used in a wide range of applications, as drug delivery systems contrast agents in magnetic resonance imaging and for hyperthermia treatments; in the production of magnetic inks or magnetic seals in motors, to name a few.[5] In the agricultural

42 scenario, the effects of iron nanoparticles have been observed in the uptake, transport,

43 accumulation and development of plant species. It was previously demonstrated that these

44 nanoparticles accumulate in pumpkin plants tissues,[6] stimulate the development of peanut[7] and

45 watermelon[8] seedlings, but did not affect growth and chlorophyll content of lettuce.[9] In all

46 instances, iron nanoparticle effects vary according to their chemical composition, size,

47 morphology, aggregation state, applied concentration as well as experimental conditions like

48 temperature and time of exposure.

49 Magnetite nanoparticles are prone to aggregation due to a combined effect of their high

50 surface area to volume ratio and their strong magnetization, thus limiting their use for bio-

51 applications.[10] To address the former problem, magnetite nanoparticles are usually synthesised

52 in the presence of surfactants, which form a coating layer preventing aggregation. Common

53 surfactants are polyethylene glycol (PEG), polyvinyl alcohol (PVA), Polyvinylpyrrolidone

54 (PVP), poly lactic-co-glycolic acid (PLGA), chitosan and dextran.[11] Among them, PEG is a

55 hydrophilic polymer widely used for biomedical applications, being biocompatible, non-

56 immunogenic, and non-antigenic.[12]

57 In this work, we report the effect of Fe_3O_4-PEG and bare Fe_3O_4 nanoparticles on the

58 germination and seedling development of *Phaseolus vulgaris* L. (common bean) seeds. The

59 effects of 1, 10, 100 and 1 000 mg Fe L^{-1} seed soaking treatments was observed on the

60 germination rate, radicle elongation and α-amylase activity of 5-days old seedlings. X-ray

61 fluorescence spectroscopy (XRF) and X-ray tomography uncovered the Fe uptake and spatial

62 distribution.

63

64 **MATERIALS AND METHODS**

65 **Synthesis of Iron Oxide Nanoparticles.** Bare magnetite nanoparticles (nFe_3O_4) were

66 synthetized by a co-precipitation method using a mixture of iron (III) chloride tetrahydrate

3

67 (FeCl$_2$·4H$_2$O) and iron (II) chloride hexahydrate (FeCl$_3$·6H$_2$O), both purchased from Sigma-

68 Aldrich, at a 2:1 molar ratio of Fe^{3+}:Fe^{2+}, m_{FeCl3} = 7.00 g, m_{FeCl2} = 2.58 g in 300 ml DI water.

69 The solution was poured in a three-neck round bottom flask provided with a condenser, nitrogen

70 and liquid inlets. Then 0.5 ml of a 37 % wt. HCl were added under gentle agitation. Oxygen

71 was purged using nitrogen for 20 minutes prior the addition of 100 ml 1.5 M NH$_4$OH. The

72 solution quickly turned black, indicating the beginning of the production of the nanoparticles.

73 The reaction lasted 1 h at 20 ˚C and nitrogen was supplied during the whole reaction. After the

74 synthesis, the nanoparticles were washed using cycles of deoxygenated DI water and magnetic

75 decantation. Then, the nanoparticles were dried at room temperature under vacuum for 24 h

76 and immediately characterized.

77 A slightly modified procedure was used to produce Fe$_3$O$_4$-PEG nanoparticles (nFe$_3$O$_4$-PEG),

78 which consisted in dissolving the iron salts in 300 ml of a 10 % wt PEG (M_w 10 000) in DI

79 water solution prior the addition of NH$_4$OH. Reaction and washing conditions were the same

80 as described above.

81 **Characterization of Pristine Fe$_3$O$_4$ Nanoparticles and Dispersions.** The composition of

82 each set of nanoparticles was determined by energy dispersive X-ray fluorescence spectroscopy

83 (EDXRF; EDX-720 Shimadzu, Japan). The quantification was carried out using the

84 fundamental parameters method (see the Supporting Information). Crystal size and phase

85 identification were determined by X-ray diffraction (XRD), using a Bruker D8-Advance

86 diffractometer (Bruker-AXS GmbH, Karlsruhe, Germany) with Cu Kα radiation.

87 Measurements were recorded for 2θ values from 20 to 80˚. Nanoparticle size and morphology

88 were evaluated via transmission electron microscopy (TEM; JEOL, JEM-2100 Plus, USA). The

89 coated and uncoated magnetite nanoparticles were suspended in deionized water and dispersed

90 using an ultrasonic processor (model 705 Sonic Dismembrator, Fisher Scientific, USA) under

91 50% amplitude for 15 min, with 30 s interval every minute, at 1, 10, 100 and 1 000 mg Fe L^{-1}.

92　The hydrodynamic size and the zeta potential of the nanomaterials at 100 mg Fe L^{-1} were

93　analyzed via dynamic light scattering (DLS; Zetasizer Nano, Malvern Instruments, UK).

94　**Germination Assay.** The effects of nFe_3O_4 and nFe_3O_4-PEG on the germination of *Phaseolus*

95　*vulgaris* L. seeds were evaluated. Since one-third of the Fe atoms in magnetite occurs as Fe^{2+}

96　and two-thirds occurs as Fe^{3+},[13] an iron ionic reference treatment (herein referred as soluble-

97　Fe) was prepared as a mixture of one-third of $FeSO_4.7H_2O$ and two-thirds of $Fe_2(SO_4)_3.nH_2O$,

98　both purchased from Reagen (Brazil).

99　*Phaseolus vulgaris* L. seeds, cultivar Sintonia, were supplied by the Agronomic Institute of

100　Campinas (IAC), presented an average germination rate of 80%. This seed was chosen as model

101　species because it has low dormancy, it results in a plant of small size and short growth cycle,

102　making it an ideal test case. In addition, *P. vulgaris* is an important and accessible source of

103　protein.[14]

104　Seeds were first immersed in a 10% NaClO solution under stirring for 10 s for disinfection,

105　followed by rinsing with deionized water. Subsequently, twenty seeds were soaked for 20 min

106　in the appropriate concentration of nFe_3O_4 and nFe_3O_4-PEG dispersions. Soluble-Fe solutions

107　at the same concentrations were used as a positive control, whereas deionized water was used

108　as a negative control. After exposure, the seeds were placed on a 15-cm paper filter fit on the

109　bottom of a Petri dish, and 8 mL of the soaking solution was added to moisturize the paper

110　filter. The Petri dishes were sealed with Parafilm M (Bemis Company Inc., USA), inserted into

111　a plastic bag to prevent water loss, and finally incubated in a germination chamber (TE-4020,

112　Tecnal, BR) under dark and ventilation at 27 °C for five days. The experiment was conducted

113　in five replicates per treatment.

114　After five days of the sowing, the assay was completed and the number of germinated seeds

115　was counted to determine the rate of germination. The radicle length of the seedlings was

116　measured, manually removed and weighted. After that, both radicles and seeds were rinsed with

117   deionized water to remove the surface-bound metal or nano metal oxide and then dried in a

118   laboratory oven (515/4A, FANEM, Brazil) at 60 °C for two days.

119   **Radicle Length Determination.** At the end of the germination period, the five replicates of

120   seedlings from each treatment were separately transferred to a black cardboard, then a HP

121   Scanjet 2410 scanner operated by Photosmart software was used to obtain scanned images of

122   the seedlings. The radicle length (cm) of the seedlings was determined through the digitized

123   images using the Seed Vigor Imaging System software (SVIS®).[15]

124   **Iron Uptake Quantification.** Replicates from each treatment were grouped and the dried

125   seedlings were carefully separated in three fractions: cotyledon, seed coat and radicle. The

126   cotyledons were then ground using a mortar mill (MA890, Marconi, Brazil). One gram of each

127   component was weighed in a decontaminated porcelain crucible and then digested by dry ashing

128   method using a muffle furnace (F-2, Fornitec, Brazil) at 100 °C h^{-1} ramp rate up to 550°C and

129   then ashed for 14 h. Each dry ashing digestion batch included a blank to ensure no

130   contamination. The ashes were dissolved in 5 mL of 1 M HNO$_{3(aq)}$, then 200 μL of this solution

131   plus 750 μL of ultrapure water was transferred into a 1.5 mL vial, and 50 μL of 1 000 mg Ga

132   L^{-1} was added as an internal standard. Then, the sample was homogenized using a tube shaker

133   vortex (MA162, Marconi, Brazil).

134   The Fe content of the digested samples was determined by EDXRF. For that, 10 μL of the

135   digests were pipetted on the external side of the window of a 6.3 mm XRF sample cup (no.

136   3577 - Spex Ind. Inc., USA) and sealed with a 5 μm thick polypropylene film (no. 3520 - Spex

137   Ind. Inc., USA). The cups were then left dry in a laboratory oven at 60°C. The samples were

138   analyzed in triplicate using a rhodium (Rh) X-ray tube at 50 kV and auto-tunable current with

139   a deadtime at 30% and a 3-mm collimator. The X-ray spectrum of the sample was acquired

140   utilizing a Si (Li) detector for 200 s. The quantification was performed using external standard

141   calibration. The trueness of this method was assessed analyzing two certified reference

142   materials: apple leaves (NIST 1515) and peach leaves (NIST 1547).

143   **Mapping Fe Accumulation Spots.** The seeds were exposed to nFe_3O_4, nFe_3O_4-PEG and

144   soluble-Fe at 1 000 mg Fe L^{-1} for 20 min, dried at room temperature and gently cut in the middle

145   using a stainless steel blade. Subsequently, the seeds were placed on a sample holder with a

146   Kapton tape and the cotyledon's inner side exposed for analysis.

147   The microanalysis was carried out using a benchtop microprobe X-ray fluorescence

148   spectrometer (μ-XRF) system (Orbis PC EDAX, USA) operated with a Rh X-ray tube at 40 kV

149   and 300 μA, and using a 25 μm Ni filter. A polycapillary optic provided a 30 μm X-ray beam

150   spot size. The detection was carried out by a 30 mm^2 silicon drift detector (140 eV FWHM at

151   the 5.9 keV Mn-Kα line) with a deadtime of nearly 3%. Maps were registered using a matrix

152   of 64x50 pixels (number of analyzed points on xy- axes) and dwell time per pixel of 1 s. The

153   experimental setup is illustrated in Figure S1 of the Supporting Information.

154   **3D Distribution of Fe in the Hilum.** Common beans have a hilum associated to the seed

155   coat, and near the hilum there is the micropyle, a small pore that allows water uptake into the

156   seed.[16] We employed X-ray tomography to verify the 3D distribution of Fe in the hilum region

157   of treated seeds.

158   Common bean seeds were exposed to nFe_3O_4-PEG and soluble-Fe at 1 000 mg Fe L^{-1} for 20

159   min and dried at room temperature. A small fraction of the seed coat containing the hilum were

160   carefully collected and cut using a razor blade.

161   Tomograms were acquired at the X-ray imaging beamline (IMX) at the 1.37 GeV Brazilian

162   Synchrotron Light Laboratory (LNLS, Campinas, Brazil). At IMX beamline, synchrotron

163   radiation was generated by a bending-magnet. The measurements were carried out using a pink

164   beam from 4 to 14 keV and 1024 projections were taken under 180º rotation. The exposure time

165   was 300 ms per projection. The image was magnified and focused on a cooled camera detector

166   (CCD; PCO.2000, PCO, Germany). Pictures of the sample holders containing the seed coat

167 fractions and the experimental X-ray tomography setup are presented in Figures S2 and S3,

168 respectively, of the Supporting Information.

169 To complement this data, these samples were also submitted to μ-XRF mapping. The analysis

170 parameters and experimental setup were the same as above mentioned (mapping Fe

171 accumulation spots).

172 **Reactivity of Soluble-Fe and Magnetite Nanoparticles.** The reactivity of the soluble-Fe and

173 magnetite nanoparticles was evaluated measuring their ability to decompose H_2O_2[17] through a

174 Fenton-like reaction.[18] In a 25 mL round-bottom reaction flask, 19.5 mL of a 1 000 mg Fe L^{-1}

175 aqueous dispersion of the tested nanoparticles and soluble-Fe solution was magnetically stirred.

176 The flask was connected to a 25 mL graduated pipette through a silicone tube. The pipette was

177 immersed in a measuring cylinder water column. Then, 0.5 mL of 30% v/v H_2O_2 solution was

178 inserted in the reaction flask with a syringe. The volume of the produced O_2 was monitored by

179 following the shift of a water column in pipette (see experimental setup at Figure S4 of the

180 Supporting Information).

181 **α-amylase Activity.** The evaluations for the α-amylase enzyme followed the recommendations

182 of Fuwa.[19] *P. vulgaris* seeds were soaked in nFe_3O_4, nFe_3O_4-PEG and soluble-Fe at 1 000 mg

183 Fe L^{-1} for 20 min and then germinated in paper rolls inside a germination chamber

184 (Mangelsdorf, DeLeo, Brazil) at 25°C. The experiment was conducted in quadruplicate, with

185 20 seeds per replicate. The seedlings were collected on the 7th day after sowing, subsequently

186 nearly 1 g were weighed and macerated using a mortar and pestle in a phosphate buffer solution

187 (pH 6.9) at a 9:1 (distilled water: buffer) ratio. This material was centrifuged for 4 min at 12

188 000 g (NT 805, Novatecnica, Brazil), then the supernatant was removed for the enzymatic

189 analysis, and 1% starch solution was used as the substrate. The value of 1 U (Enzymatic Unit)

190 was considered to be the reduction of 10% of the colorimetric intensity of the amylose-iodine

191 complex.

192   **Statistical Analysis.** The number of germinated seeds and the radicle length and weight data

193   were submitted to analysis of variance (ANOVA) and Tukey's multiple range tests at 95%

194   confidence interval using the Action Stat software (version 3.3.111.1178, Estatcamp, BR).

195

196   **RESULTS AND DISCUSSION**

197   **Characterization of the Nanoparticles and Dispersions.** The purity of the nFe_3O_4 and

198   Fe_3O_4-PEG was determined by EDXRF. Considering the limits of detection of the method, in

199   the order of mg kg^{-1}, no contaminants were found in the nanoparticles. Figure S5 in the

200   Supporting Information presents the XRF spectra for these samples. XRD patterns, presented

201   in Figure S6, showed that the average crystallite size in the direction of the plane (220) were

202   11.6 and 13.9 nm for the uncoated and coated magnetite nanoparticles, respectively (see the

203   crystallite size in the direction of the other planes in Table S1 of the Supporting Information).

204   These results were in good agreement with the observations by transmission electron

205   microscopy (TEM) (Figure S7), which presumed an average particle size of 11 nm for nFe_3O_4

206   and 12 nm for Fe_3O_4-PEG.

207   The DLS measurements (Table 1) revealed that in aqueous dispersions the nanoparticles

208   used for seed priming formed aggregates (DLS curves are in Figure S8). The values are in broad

209   agreement with reported values of 208 ± 15 nm for 50-60 nm nFe_3O_4 suspended in water at 10

210   mg L^{-1} and 438 ± 13 nm at 20 mg L^{-1}.[9] One could visually observe that such aggregates make

211   these magnetite dispersions very unstable. At 1 000 mg Fe L^{-1}, most was settled after 60 min,

212   and even in the nFe_3O_4-PEG case. Zeta-potential measurements indicated that the uncoated

213   magnetite presented a negative value, while the PEG coated had a positive result. The pH

214   registered for the uncoated magnetite dispersion used in these analyses was 5.58 and 5.08 for

215   the PEG coated dispersion. A possible explanation to the former behavior is the steric hindrance

216   over the surface active sites produced by the adsorption of polymers with high molecular

9

217 weight, such as PEG.[20] The measured ζ-potential for the uncoated samples was different from

218 values reported in the literature, 4.31 ± 0.05 mV for the less concentrated dispersion (10 mg L$^-$

219 ^{1}) and 3.99 ± 0.4 mV for the highest one (20 mg L^{-1}).[9]

220 **Effects of Magnetite Nanoparticles on *P. vulgaris* Seed Germination and Radicle**

221 **Growth.** The number of germinated seeds was daily counted and all the radicles emerged

222 almost in the same period. At the end of the germination assay, the deionized water treatment

223 control gave an average germination rate of 88.8% (Figure 1). All the others treatments had

224 higher or comparable values to the negative control. The highest germination rate was found

225 for 1 mg Fe L^{-1} of nFe$_3$O$_4$ and 10 mg Fe L^{-1} of nFe$_3$O$_4$-PEG (97 and 96%, respectively).

226 However, under ANOVA statistical analysis, no difference was found among treatments and

227 controls ($p < 0.05$).

228 Although the treatments did not affect the germination rate, a different scenario was

229 observed in the radicle elongation of the seedlings. The phenotypic images of the seedlings

230 after 5 days of Fe treatments exposure (Figure 2) indicate that the highest applied concentration

231 was toxic for the seedlings development, but this was not observed for the nFe$_3$O$_4$-PEG

232 treatment.

233 The average length of the radicle of negative control was 5.9 ± 1.0 cm long, whilst nFe$_3$O$_4$

234 and soluble-Fe at 1 000 mg Fe L^{-1} shortened it yielding 2.9 ± 0.5 and 1.2 ± 0.3 cm, respectively.

235 Conversely, PEG improved the radicle development even at its higher concentration, where the

236 highest radicle elongation of 8.1 ± 1.1 cm was observed (Figure 3a). This effect can be

237 attributed to the hydrophilic nature of the PEG,[21] which may have aided in root growth by

238 redirecting water to a region close to the root of the seedlings, an effect caused by the reduction

239 of water potential, thus determining greater water absorption by the tissue and consequently its

240 growth. In addition, the distribution of nanoparticles on seed coat were more homogeneous

241   when PEG was added. This led to a controlled absorption of nFe_3O_4, by the reduction of the

242   water surface tension.[22]

243   After the length measurements, the radicles were removed and weighed (Figure 3b). The same

244   trend was observed for length and weight, radicles from water treatment presented 1.94 ± 0.13

245   g and nFe_3O_4 at 1 000 mg Fe L^{-1} had 0.82 ± 0.09 g. According to the Tukey's test ($p < 0.05$),

246   radicle length was significantly different from the control at 1 000 mg Fe L^{-1} for all the tested

247   materials, positively for nFe_3O_4-PEG and negatively for nFe_3O_4 and soluble-Fe treatments

248   (Figure S9). However, radicle weight data was only statistically different from control for

249   nFe_3O_4 and soluble-Fe at 1 000 mg Fe L^{-1} (Figure S10).

250   The phytotoxicity observed for high concentrations of soluble-Fe and nFe_3O_4 might be related

251   to the accumulation of this element in the seed tissues. Such statement is reinforced by fact that

252   the absorption of soluble-Fe occurs mainly by the micropyle, the determinant structure for water

253   imbibition by seeds,[23] mainly in the initial stages of the germination process, as will be

254   discussed in depth bellow.

255   Studies reported root shortening as the concentration of nanoparticle in the dispersion

256   increases. This was demonstrated for ZnO,[24, 25] Ag,[26] CuO[27, 28] and TiO_2.[29] The anomalous

257   behavior found for Fe in the present study was also observed for white mustard, where the root

258   elongation of the seedlings treated with the highest nFe_3O_4 concentrations (100 and 1 000 mg

259   L^{-1}) was higher than the lower tested concentration (10 mg L^{-1}), although the difference was

260   not statistically significant.[30] On the other hand, soybean and rice seeds treated with γ-Fe_2O_3

261   nanoparticles at 500, 1 000 and 2 000 mg L^{-1} developed seedlings with the root elongation

262   significantly higher than the control.[31, 32]

263   Nano zerovalent iron at 5 000 mg L^{-1} also promoted the root elongation of *Arabidopsis*

264   *thaliana* by 150-200% compared to the control, with the elongation caused by hydroxyl radical-

265   induced cell wall loosening.[33] Other authors observed that γ-Fe_2O_3 nanoparticles promoted the

266 growth of peanut by regulating the antioxidant enzyme activity and the content of abscisic acid,

267 a phytohormone that stimulates the senescence and reduces the metabolism. The peanut root

268 dry biomass was increased by Fe_2O_3 nanoparticles at 1 000 mg kg^{-1} applied to the soil.[34]

269   Since PEG is hydrophilic, it can prevent the nFe_3O_4-PEG from interacting with cells and/or

270 proteins.[12] In animal cells, the surface chemistry modification of iron oxide nanoparticles by

271 PEG reduced the cytotoxicity and the formation of reactive oxygen species (ROS), with the cell

272 length not affected compared to those treated with bare nanoparticles.[35] The uptake of PEG-

273 coated magnetite by macrophage cells was much lower than that of uncoated nanoparticles.[36,

274 37]

275 **Determination of Fe uptake by *P. vulgaris* seeds.** After the germination assays, the seedling

276 tissues were divided and the Fe content was determined. These tissues are presented in the

277 Figure S11 of the Supporting Information. Figure 4 presents the concentration of Fe in the (a)

278 seed coat, (b) cotyledon and (c) radicle of the seedlings exposed to nFe_3O_4, nFe_3O_4-PEG,

279 soluble-Fe and water negative control.

280   The negative control (deionized water) revealed that Fe is more concentrated in the seed coat

281 of the tested common beans than in the others tissues analyzed. It presented 92.3 ± 0.6 mg Fe

282 kg^{-1}, in contrast to 46.6 ± 1.4 mg Fe kg^{-1} in the cotyledons and 72.8 ± 0.5 mg Fe kg^{-1} in the

283 radicle. In the case of the seedlings that received nanoparticle treatment, those that were soaked

284 in nFe_3O_4 presented similar Fe content in the three analyzed regions, regardless of the applied

285 concentration. The difference between the water control and nFe_3O_4 treatment reached a

286 maximum value of 50% in the seed coat sample that was soaked in 1 000 mg Fe L^{-1}, while this

287 difference was more than 6 000-fold higher for the soluble-Fe treatment. At the highest

288 treatment concentration, the incorporation of Fe from the nFe_3O_4-PEG in the seed coat and in

289 the radicle was intermediate between those of nFe_3O_4 and soluble-Fe.

290   Intending to estimate the contribution of dissolved Fe on the seedling development and Fe

291   uptake, solubility tests in deionized water were performed as described in the Supporting

292   Information. For nFe_3O_4 and nFe_3O_4-PEG dispersions at 100 and 1 000 mg Fe L^{-1}, the soluble

293   Fe fractions were not quantitatively detected, i.e. they were below the limit of quantification of

294   the method (0.15 mg Fe L^{-1}). In a study carried out by Landa et al.[30] it was found 6.51 ± 2.24

295   mg Fe L^{-1} in the supernatant of a cultivation medium supplemented with nFe_3O_4 at 1 000 mg L^{-1}

296   . However, it is important to keep in mind that the presence of other molecules can induce the

297   generation of soluble complexes with Fe.

298   Due to the low solubility, one can hypothesize that Fe was mainly taken up by the seedling

299   tissues as intact magnetite nanoparticles. These nanoparticles then could undergo dissolution

300   within the plant tissues. The chemical speciation of the incorporated Fe will be addressed in

301   further studies.

302   **Spatial Distribution of Fe in the Primed Seeds.** Figure 5 presents the internal side of the

303   cotyledon of a *P. vulgaris* seeds soaked for 20 min in (a) nFe_3O_4-PEG and (b) soluble-Fe at 1

304   000 mg Fe L^{-1}. The results corroborate the quantitative analysis, indicating that the treatments

305   concentrated Fe in the seed coat, mainly in the hilum region, and the number of XRF counts

306   was almost 5-fold higher for the soluble-Fe treatment compared to the nanoparticle one.

307   Additional μ-XRF chemical maps were recorded specifically in the hilum region of the treated

308   seeds. The images of the Fe distribution in the hilum revealed a different pattern of distribution

309   between seeds soaked in nFe_3O_4-PEG dispersion and soluble-Fe solution at 1 000 mg Fe L^{-1}

310   (Figure 6). The nanoparticle treatment concentrated Fe mainly in the edge around the hilum

311   (Figure 6a), while soluble-Fe presented a hotspot in the micropyle (Figure 6b). Other study[38]

312   using magnetic resonance microscopy showed that during the imbibition process, water enters

313   the *P. vulgaris* seed through the micropyle, and consequently, this is the channel for soluble Fe

314   ions.

315 The hilum is a sponge-like tissue (see Figure S12 in the SI), thus besides sticking on the

316 tissue's outer surface, the nanoparticles can penetrate through the channels reaching internal

317 layers. In spite of X-ray fluorescence's high analytical sensitivity, it yielded only 2D maps. The

318 6.4 keV Kα photons emitted by Fe atoms embedded in the seed coat can escape from a depth

319 that lies in the mm range. As such, the images shown in Figure 6 cannot tell whether Fe is only

320 adsorbed on the surface of the seed coat or whether it was also inside the hilum tissue.

321 Hence, the hilum region of treated seeds was subjected to further X-ray tomography analysis.

322 Figure 7 shows 3D projections and slices of phase contrast tomography for the seed coat of

323 seeds soaked in (a) nFe$_3$O$_4$-PEG and (b) soluble-Fe at 1 000 mg Fe L^{-1} for 20 min. The greenish

324 regions, highlighted by the red circles, indicate the presence of Fe that penetrated within the

325 hilum sponge tissue. This can be observed for both nFe$_3$O$_4$-PEG and soluble-Fe. The

326 combination of μ-XRF and X-ray tomography unequivocally showed that Fe supplied in

327 nanoparticulate form could enter in the seeds.

328 X-ray tomography was previously employed to understand physiological seed development

329 of rice,[39] maize[40] and oilseed rape,[41] observe germination behavior of sugar beet seeds,[42] and

330 also to analyze archaeological seeds in the investigation of crop domestication.[43, 44] However,

331 to the best of our knowledge, no other study examined 3D images of a nanoparticle-treated bean

332 seed, although some researchers used this technique to verify the uptake and distribution of

333 gold and yttrium nanoparticles in *Arabidopsis thaliana*[45] and cabbage plants.[46]

334 **Chemical Reactivity of nFe$_3$O$_4$ and nFe$_3$O$_4$-PEG.** The chemical reactivity of the tested

335 materials was accessed through the volume of O$_2$ produced during the degradation of H$_2$O$_2$ by

336 the magnetite nanoparticles and soluble-Fe used for seed soaking. The most reactive

337 nanoparticle was nFe$_3$O$_4$ which produced 12.4 mL of O$_2$ in 300 min, while nFe$_3$O$_4$-PEG

338 produced 7.5 mL in the same time. On the other hand, soluble-Fe readily produced 22.1 mL in

339 8 min (Figure S13). Iron catalyzes the decomposition of H$_2$O$_2$ trough Fenton reaction. The high

340 reactivity of the soluble-Fe is due to the availability of free ionic Fe that leads to homogenous

341 Fenton reaction, which is faster than the heterogeneous one.[47] On the other hand, the lower

342 reactivity of the PEG coated nanoparticles may be the result of a lower number of available Fe

343 sites, since the nanoparticle surface is sterically hindered by the polymeric chains. This result

344 may explain the non-deleterious effects caused by the coated nanoparticles in the radicle

345 elongation, even at high concentrations.

346 **α-amylase Activity.** The energy source necessary for the germination and early seedling

347 development of leguminous comes mainly from the degradation of proteins and carbohydrates

348 present in the seed reserves. Protein and starch comprise about 20% and 40% of the whole *P.*

349 *vulgaris* seed, respectively.[48] Here we evaluated the α-amylase (starch degrading enzyme)

350 activity in the seedlings whose seeds were soaked in nFe_3O_4, nFe_3O_4-PEG and soluble-Fe at 1

351 000 mg Fe L^{-1}.

352 Compared to the result that was obtained for the non-treated seeds (1600 ± 300 U), soluble-

353 Fe treatment presented the lowest enzymatic activity, followed by nFe_3O_4 (730 ± 30 and 760 ±

354 140 U, respectively). Reinforcing what was observed in the radicle development and in the

355 chemical reactivity analysis, nFe_3O_4-PEG treatment was the least harmful to the α-amylase

356 activity (900 ± 180 U) (Table S2).

357 α-amylase is a metalloenzyme which needs Ca^{2+} to its activity and stability, its affinity is

358 much stronger than that with others ions.[49] Since Fe^{2+} is also a divalent ion, its presence in

359 abundance could provoke a competition with Ca^{2+} during the α-amylase biosynthesis, leading

360 to enzymatic activity loss. This possibility is supported by the previously observed reduction

361 of amylase activity *in vitro* in fish intestine after Fe^{2+} addition (50 mg kg^{-1}).[50]

362 Figure S14 attempts to correlate the radicle length and weight to the content of Fe

363 incorporated by the seedling tissues. Although the Fe amount in the seedling tissues was very

364 similar, the biologic effects were distinct: The deleterious effects caused by 1 000 mg Fe L^{-1}

15

soluble-Fe can be attributed to phytotoxicity due the excess of this element, as previously discussed. However, the growth promotion induced by nFe$_3$O$_4$-PEG cannot be explained solely by the content of Fe incorporated by the seedlings. Since the highest seedling growth and weight gain were observed for the nFe$_3$O$_4$-PEG, and this treatment did not yield the highest α-amylase activity, one can infer that the decomposition of starch was not the limiting factor for the seedling development.

We previously demonstrated that Cu from CuO nanoparticles were mostly concentrated in the seed coat of *P. vulgaris* seeds after soaking, especially in the hilum region,[28] but now thanks to X-ray microtomography we concluded that Fe from magnetite nanoparticles was not only absorbed on the surface of the seed coat, but also penetrated the hilum tissue, an evidence that nanoparticles can enter in the seeds.

Although the root elongation and shortening caused by nanoparticles seed treatment were already demonstrated for cucumber treated with ZnO[25] and CuO,[51] corn soaked in ZnO,[25] mung bean exposed to Ag,[26] and even for white mustard treated with magnetite nanoparticle,[30] nothing was reported so far about the influence of coated nanoparticle on the root length. Even though the mechanisms involved in this phenomenon is not well understood, the literature states that nanoparticles can penetrate root cells membranes, enhance water uptake and consequently induce the root elongation.[52]

The presented paper also highlighted that the PEG coating turn the nanoparticles less reactive than uncoated one. It was already demonstrated that surfactant coated nanoparticles can be less toxic than their uncoated counterparts.[53, 54] Besides the PEG coating, the radicle growth can be also related to an intermediated content of Fe uptake by the radicles. As above mentioned, the radicle elongation for other plant species also increased as the applied Fe nanoparticle concentration raised.[30-32]

Altogether, the results showed that nanomaterials are potential candidates for seed priming.

390 The deleterious effects of magnetite nanoparticles were smaller than those shown by aqueous

391 Fe^{3+}/Fe^{2+}. Thus, the supplying of nutrients through sources of intermediate solubility makes

392 phytotoxicity less prone to occur. Rather than only transferring nutrients to the roots, X-ray

393 fluorescence and tomography showed that the nanoparticles can penetrate within the seed

394 structure and thus modify the seedling development. Finally, the PEG coating played a major

395 role on the properties of the magnetite nanoparticles and might be responsible for the growth

396 promotion reported in this study.

397

ABBREVIATIONS USED

398		
399	Fe$_3$O$_4$	magnetite
400	PEG	polyethylene glycol
401	PVA	polyvinyl alcohol
402	PVP	polyvinylpyrrolidone
403	PLGA	poly lactic-co-glycolic acid
404	XRF	X-ray fluorescence spectroscopy
405	nFe$_3$O$_4$	magnetite nanoparticles
406	nFe$_3$O$_4$-PEG	magnetite nanoparticles covered with polyethylene glycol
407	FeSO$_4$.7H$_2$O	iron(II) sulfate heptahydrate
408	Fe$_2$(SO$_4$)$_3$.nH$_2$O	iron(III) sulfate hydrate
409	EDXRF	energy dispersive X-ray fluorescence spectroscopy
410	XRD	X-ray diffraction
411	TEM	transmission electron microscopy
412	DLS	dynamic light scattering
413	LNBio	Brazilian Biosciences National Laboratory
414	IAC	Agronomic Institute of Campinas
415	NaClO	sodium hypochlorite
416	SVIS$^®$	Seed Vigor Imaging System
417	LPV	Department of Crop Science
418	ESALQ	"Luiz de Queiroz" College of Agriculture
419	USP	University of São Paulo
420	ANOVA	analysis of variance
421	HNO$_3$	nitric acid
422	μ-XRF	micro probe X-ray fluorescence spectroscopy

423   IMX   X-ray imaging beamline

424   LNLS   Brazilian Synchrotron Light Laboratory

425   CCD   cooled camera detector

426   H_2O water

427   H_2O_2 hydrogen peroxide

428   U   Enzymatic Unit

429   ZnO   zinc oxide

430   CuO   copper(II) oxide

431   TiO_2 titanium dioxide

432   Fe_2O_3 maghemite

433   ROS   reactive oxygen species

434

448 **SUPPORTING INFORMATION**

449 The Supporting Information is available free of charge on the ACS Publications website at DOI:

450 Purity and contaminant analysis of nFe_3O_4 and Fe_3O_4-PEG (EDXRF methodology and spectra);

451 XRD analysis methodology, diffractograms and crystallite size of the magnetite nanoparticles;

452 μ-XRF experimental setup; X-ray tomography imaging experimental setup; Experimental

453 setup and results for the nFe_3O_4 and Fe_3O_4-PEG reactivity analysis; TEM images of nFe_3O_4

454 and Fe_3O_4-PEG; DLS curves; Statistical analysis (Tukey test); Pictures of the three fractions of

455 the seedlings (seed coat, cotyledon and radicle) analyzed by EDXRF; methodology and

456 quantitative results of the solubility tests carried out with the nFe_3O_4 and Fe_3O_4-PEG

457 dispersions; SEM image of the hilum of a *P. vulgaris* seed; α-amylase activity in the

458 germinated treated beans; Correlation between radicle length and weight with the content

459 of Fe incorporated by the seedling tissues (seed coat, cotyledon and radicle).

460

461 **REFERENCES**

462

463 (1) Raliya, R.; Saharan, V.; Dimkpa, C.; Biswas, P. Nanofertilizer for precision and

464 sustainable agriculture: current state and future perspectives. *J. Agric. Food Chem.* **2017**, DOI:

465 10.1021/acs.jafc.7b02178.

466 (2) Marschner, P. *Mineral Nutrition of Higher Plants*. 3rd. ed.; Academic Press: San Diego,

467 2012; 672 pages.

468 (3) Schwertmann, U. Solubility and dissolution of iron-oxides. *Plant Soil* **1991,** *130*, 1-25.

469 (4) Romheld, V.; Marschner, H. Evidence for a specific uptake system for iron

470 phytosiderophores in roots of grasses. *Plant Physiol.* **1986**, *80*, 175-180.

471   (5) Figuerola, A.; Di Corato, R.; Manna, L.; Pellegrino, T. From iron oxide nanoparticles

472   towards advanced iron-based inorganic materials designed for biomedical applications.

473   *Pharmacol. Res.* **2010,** *62*, 126-143.

474   (6) Zhu, H.; Han, J.; Xiao, J. Q.; Jin, Y. Uptake, translocation, and accumulation of

475   manufactured iron oxide nanoparticles by pumpkin plants. *J. Environ. Monitor.* **2008,** *10*, 713-

476   717.

477   (7) Li, X.; Yang, Y. C.; Gao, B.; Zhang, M. Stimulation of peanut seedling development and

478   growth by zero-valent iron nanoparticles at low concentrations. *Plos One* **2015,** *10*, 12.

479   (8) Li, J. L.; Chang, P. R.; Huang, J.; Wang, Y. Q.; Yuan, H.; Ren, H. X. Physiological effects

480   of magnetic iron oxide nanoparticles towards watermelon. *J. Nanosci. Nanotechno.* **2013,** *13*,

481   5561-5567.

482   (9) Trujillo-Reyes, J.; Majumdar, S.; Botez, C. E.; Peralta-Videa, J. R.; Gardea-Torresdey, J. L.

483   Exposure studies of core-shell Fe/Fe_3O_4 and Cu/CuO NPs to lettuce (*Lactuca sativa*) plants:

484   Are they a potential physiological and nutritional hazard? *J. Hazard. Mater.* **2014,** *267*, 255-

485   263.

486   (10) Gupta, A. K.; Gupta, M. Synthesis and surface engineering of iron oxide nanoparticles for

487   biomedical applications. *Biomaterials* **2005,** *26*, 3995-4021.

488   (11) Laurent, S.; Forge, D.; Port, M.; Roch, A.; Robic, C.; Elst, L. V.; Muller, R. N. Magnetic

489   iron oxide nanoparticles: Synthesis, stabilization, vectorization, physicochemical

490   characterizations, and biological applications. *Chem. Rev.* **2008,** *108*, 2064-2110.

491   (12) Gupta, A. K.; Wells, S. Surface-modified superparamagnetic nanoparticles for drug

492   delivery: preparation, characterization, and cytotoxicity studies. *IEEE Trans. NanoBiosci.*

493   **2004,** *3*, 66-73.

494   (13) Yamashita, T.; Hayes, P. Analysis of XPS spectra of Fe^{2+} and Fe^{3+} ions in oxide materials.

495   *Appl. Surf. Sci.* **2008,** *254*, 2441-2449.

496 (14) Rossi, G. B.; Valentim-Neto, P. A.; Blank, M.; de Faria, J. C.; Arisi, A. C. M. Comparison

497 of grain proteome profiles of four brazilian common bean (*Phaseolus vulgaris* L.) cultivars. *J.*

498 *Agric. Food Chem.* **2017,** *65*, 7588-7597.

499 (15) Sako, Y.; McDonald, M. B.; Fujimura, K.; Evans, A. F.; Bennett, M. A. A system for

500 automated seed vigour assessment. *Seed Sci. Technol.* **2001**, *29*, 625-636.

501 (16) Vieira, C.; Paula Júnior, T. J.; Borém, A. Botânica. In *Feijão*. 2 ed.; Universidade Federal

502 de Viçosa: Viçosa, Brazil, 2006; 600 pp.

503 (17) Silva, A. C.; Oliveira, D. Q. L.; Oliveira, L. C. A.; Anastacio, A. S.; Ramalho, T. C.; Lopes,

504 J. H.; Carvalho, H. W. P.; Torres, C. E. R. Nb-containing hematites $Fe_{2-x}Nb_xO_3$: The role of

505 Nb^{5+} on the reactivity in presence of the H_2O_2 or ultraviolet light. *Appl. Catal. a-Gen.* **2009,**

506 *357*, 79-84.

507 (18) Carvalho, H. W. P.; Hammer, P.; Pulcinelli, S. H.; Santilli, C. V.; Molina, E. F.

508 Improvement of the photocatalytic activity of magnetite by Mn-incorporation. *Mater. Sci. Eng.*

509 *B-Solid.* **2014,** *181*, 64-69.

510 (19) Fuwa, H. A new method for microdetermination of amylase activity by the use of amylose

511 as the substrate. *J. Biochem.* **1954,** *41*, 583-603.

512 (20) Liufu, S.; Xiao, H.; Li, Y. Investigation of PEG adsorption on the surface of zinc oxide

513 nanoparticles. *Powder Technol.* **2004,** *145*, 20-24.

514 (21) Thijs, H. M. L.; Becer, C. R.; Guerrero-Sanchez, C.; Fournier, D.; Hoogenboom, R.;

515 Schubert, U. S. Water uptake of hydrophilic polymers determined by a thermal gravimetric

516 analyzer with a controlled humidity chamber. *J. Mater. Chem.* **2007,** *17*, 4864-4871.

517 (22) Schwuger, M. Mechanism of interaction between ionic surfactants and polyglycol ethers

518 in water. *J. Colloid Interf. Sci.* **1973,** *43*, 491-498.

519 (23) Das, B.; Saha, P. K. Ultrastuctural dimorphism of micropyle determines differential

520 germinability of *Sesbania cannabina* seeds. *Seed Sci. Technol.* **2006,** *34*, 363-372.

521 (24) Lin, D. H.; Xing, B. S. Phytotoxicity of nanoparticles: Inhibition of seed germination and

522 root growth. *Environ. Pollut.* **2007,** *150*, 243-250.

523 (25) Zhang, R. C.; Zhang, H. B.; Tu, C.; Hu, X. F.; Li, L. Z.; Luo, Y. M.; Christie, P.

524 Phytotoxicity of ZnO nanoparticles and the released Zn(II) ion to corn (*Zea mays* L.) and

525 cucumber (*Cucumis sativus* L.) during germination. *Environ. Sci. Pollut. R.* **2015,** *22*, 11109-

526 11117.

527 (26) Nair, P. M. G.; Chung, I. M. Physiological and molecular level studies on the toxicity of

528 silver nanoparticles in germinating seedlings of mung bean (*Vigna radiata* L.). *Acta Physiol.*

529 *Plant.* **2015,** *37*, 11.

530 (27) Adams, J.; Wright, M.; Wagner, H.; Valiente, J.; Britt, D.; Anderson, A. Cu from

531 dissolution of CuO nanoparticles signals changes in root morphology. *Plant Physiol. Bioch.*

532 **2017,** *110*, 108-117.

533 (28) Duran, N. M.; Savassa, S. M.; de Lima, R. G.; de Almeida, E.; Linhares, F. S.; van Gestel,

534 C. A. M.; de Carvalho, H. W. P. X-ray spectroscopy uncovering the effects of Cu based

535 nanoparticle concentration and structure on *Phaseolus vulgaris* germination and seedling

536 development. *J. Agric. Food Chem.* **2017,** *65*, 7874-7884.

537 (29) Castiglione, M. R.; Giorgetti, L.; Geri, C.; Cremonini, R. The effects of nano-TiO_2 on seed

538 germination, development and mitosis of root tip cells of *Vicia narbonensis* L. and *Zea mays*

539 L. *J. Nanopart. Res.* **2011,** *13*, 2443-2449.

540 (30) Landa, P.; Cyrusova, T.; Jerabkova, J.; Drabek, O.; Vanek, T.; Podlipna, R. Effect of metal

541 oxides on plant germination: phytotoxicity of nanoparticles, bulk materials, and metal ions.

542 *Water Air Soil Poll.* **2016,** *227*, 10.

543 (31) Alidoust, D.; Isoda, A. Effect of gamma Fe_2O_3 nanoparticles on photosynthetic

544 characteristic of soybean (*Glycine max* (L.) Merr.): foliar spray versus soil amendment. *Acta*

545 *Physiol. Plant.* **2013,** *35*, 3365-3375.

546   (32) Alidoust, D.; Isoda, A. Phytotoxicity assessment of gamma-Fe_2O_3 nanoparticles on root

547   elongation and growth of rice plant. *Environ. Earth Sci.* **2014,** *71*, 5173-5182.

548   (33) Kim, J. H.; Lee, Y.; Kim, E. J.; Gu, S.; Sohn, E. J.; Seo, Y. S.; An, H. J.; Chang, Y. S.

549   Exposure of iron nanoparticles to *Arabidopsis thaliana* enhances root elongation by triggering

550   cell wall loosening. *Environ. Sci. Technol.* **2014,** *48*, 3477-3485.

551   (34) Rui, M. M.; Ma, C. X.; Hao, Y.; Guo, J.; Rui, Y. K.; Tang, X. L.; Zhao, Q.; Fan, X.; Zhang,

552   Z. T.; Hou, T. Q.; Zhu, S. Y. Iron oxide nanoparticles as a potential iron fertilizer for peanut

553   (*Arachis hypogaea*). *Front. Plant Sci.* **2016,** *7*, 10.

554   (35) Yu, M.; Huang, S. H.; Yu, K. J.; Clyne, A. M. Dextran and polymer polyethylene glycol

555   (PEG) coating reduce both 5 and 30 nm iron oxide nanoparticle cytotoxicity in 2D and 3D cell

556   culture. *Int. J. Mol. Sci.* **2012,** *13*, 5554-5570.

557   (36) Zhang, Y.; Kohler, N.; Zhang, M. Q. Surface modification of superparamagnetic magnetite

558   nanoparticles and their intracellular uptake. *Biomaterials* **2002,** *23*, 1553-1561.

559   (37) Xie, J.; Xu, C.; Kohler, N.; Hou, Y.; Sun, S. Controlled PEGylation of monodisperse Fe_3O_4

560   nanoparticles for reduced non-specific uptake by macrophage cells. *Adv. Mater.* **2007,** *19*,

561   3163-3166.

562   (38) Mikac, U.; Sepe, A.; Sersa, I. MR microscopy for noninvasive detection of water

563   distribution during soaking and cooking in the common bean. *Magn. Reson. Imag.* **2015,** *33*,

564   336-345.

565   (39) Jhala, V. M.; Thaker, V. S. X-ray computed tomography to study rice (*Oryza sativa* L.)

566   panicle development. *J. Exp. Bot.* **2015,** *66*, 6819-6825.

567   (40) Rousseau, D.; Widiez, T.; Di Tommaso, S.; Rositi, H.; Adrien, J.; Maire, E.; Langer, M.;

568   Olivier, C.; Peyrin, F.; Rogowsky, P. Fast virtual histology using X-ray in-line phase

569   tomography: application to the 3D anatomy of maize developing seeds. *Plant Methods* **2015,**

570   *11*, 10.

571 (41) Verboven, P.; Herremans, E.; Borisjuk, L.; Helfen, L.; Ho, Q. T.; Tschiersch, H.; Fuchs,

572 J.; Nicolai, B. M.; Rolletschek, H. Void space inside the developing seed of *Brassica napus* and

573 the modelling of its function. *New Phytol.* **2013,** *199*, 936-947.

574 (42) Blunk, S.; Malik, A. H.; de Heer, M. I.; Ekblad, T.; Fredlund, K.; Mooney, S. J.; Sturrock,

575 C. J. Quantification of differences in germination behaviour of pelleted and coated sugar beet

576 seeds using x-ray computed tomography (x-ray CT). *Biomed. Phys. Eng. Express* **2017,** *3*, 11.

577 (43) Zong, Y. B.; Yao, S. K.; Crawford, G. W.; Fang, H.; Lang, J. F.; Fan, J. D.; Sun, Z. B.;

578 Liu, Y.; Zhang, J. H.; Duan, X. L.; Zhou, G. Z.; Xiao, T. Q.; Luan, F. S.; Wang, Q.; Chen, X.

579 X.; Jiang, H. D. Selection for oil content during soybean domestication revealed by X-ray

580 tomography of ancient beans. *Sci. Rep-UK* **2017,** *7*, 10.

581 (44) Murphy, C.; Fuller, D. Q. Seed coat thinning during horsegram (*Macrotyloma uniflorum*)

582 domestication documented through synchrotron tomography of archaeological seeds. *Sci. Rep-*

583 *UK* **2017,** *7*, 9.

584 (45) Avellan, A.; Schwab, F.; Masion, A.; Chaurand, P.; Borschneck, D.; Vidal, V.; Rose, J.;

585 Santaella, C.; Levard, C. Nanoparticle uptake in plants: gold nanomaterial localized in roots of

586 *Arabidopsis thaliana* by X-ray computed nanotomography and hyperspectral imaging. *Environ.*

587 *Sci. Technol.* **2017,** *51*, 8682-8691.

588 (46) Chen, Y. Y.; Sanchez, C.; Yue, Y.; de Almeida, M.; Gonzalez, J. M.; Parkinson, D. Y.;

589 Liang, H. Observation of yttrium oxide nanoparticles in cabbage (*Brassica oleracea*) through

590 dual energy K-edge subtraction imaging. *J. Nanobiotechnol.* **2016,** *14*, 10.

591 (47) Xavier, S.; Gandhimathi, R.; Nidheesh, P. V.; Ramesh, S. T. Comparison of homogeneous

592 and heterogeneous Fenton processes for the removal of reactive dye Magenta MB from aqueous

593 solution. *Desalin. Water Treat.* **2015,** *53*, 109-118.

594 (48) Marquezi, M.; Gervin, V. M.; Watanabe, L. B.; Bassinello, P. Z.; Amante, E. R. Physical

595 and chemical properties of starch and flour from different common bean (*Phaseolus vulgaris*

596 L.) cultivars. *Braz. J. Food Technol.* **2016**, 19, e2016005.

597 (49) Gupta, R.; Gigras, P.; Mohapatra, H.; Goswami, V. K.; Chauhan, B. Microbial alpha-

598 amylases: a biotechnological perspective. *Process Biochem.* **2003,** *38*, 1599-1616.

599 (50) Li, J. S.; Li, J. L.; Wu, T. T. The effects of copper, iron and zinc on digestive enzyme

600 activity in the hybrid tilapia *Oreochromis niloticus* (L.) x *Oreochromis aureus* (Steindachner).

601 *J. Fish Biol.* **2007,** *71*, 1788-1798.

602 (51) Moon, Y. S.; Park, E. S.; Kim, T. O.; Lee, H. S.; Lee, S. E. SELDI-TOF MS-based

603 discovery of a biomarker in *Cucumis sativus* seeds exposed to CuO nanoparticles. *Environ.*

604 *Toxicol. Phar.* **2014,** *38*, 922-931.

605 (52) Wang, X. P.; Han, H. Y.; Liu, X. Q.; Gu, X. X.; Chen, K.; Lu, D. L. Multi-walled carbon

606 nanotubes can enhance root elongation of wheat (*Triticum aestivum*) plants. *J. Nanopart. Res.*

607 **2012,** *14*, 10.

608 (53) Nguyen, K. C.; Seligy, V. L.; Massarsky, A.; Moon, T. W.; Rippstein, P.; Tan, J.; Tayabali,

609 A. F. Iop In *Comparison of toxicity of uncoated and coated silver nanoparticles*, 3rd

610 International Conference on Safe Production and Use of Nanomaterials (Nanosafe), Minatec,

611 Grenoble, FRANCE, Nov 13-15; Iop Publishing Ltd: Minatec, Grenoble, France, 2012.

612 (54) Suresh, A. K.; Pelletier, D. A.; Wang, W.; Moon, J. W.; Gu, B. H.; Mortensen, N. P.;

613 Allison, D. P.; Joy, D. C.; Phelps, T. J.; Doktycz, M. J. Silver Nanocrystallites: Biofabrication

614 using *Shewanella oneidensis*, and an evaluation of their comparative toxicity on gram-negative

615 and gram-positive bacteria. *Environ. Sci. Technol.* **2010,** *44*, 5210-5215.

616

FIGURE CAPTIONS

Figure 1. Germination rate of *P. vulgaris* seeds exposed to nFe_3O_4, nFe_3O_4-PEG, soluble-Fe (1, 10, 100 and 1 000 mg Fe L^{-1}) and H_2O after 5 days of germination.

Figure 2. Seedlings of *P. vulgaris* whose seeds were soaked in (a) H_2O, (b) nFe_3O_4, (c) nFe_3O_4-PEG and (d) soluble-Fe. Applied concentrations were 1, 10, 100 and 1 000 mg Fe L^{-1}.

Figure 3. (a) Radicle length and (b) weight of *P. vulgaris* seedlings whose seeds were soaked in nFe_3O_4, nFe_3O_4-PEG, soluble-Fe (1, 10, 100 and 1 000 mg Fe L^{-1}) and H_2O (control).

Figure 4. Iron concentration in the (a) seed coat, (b) cotyledon and (c) radicle of germinated *P. vulgaris* seeds soaked in nFe_3O_4, nFe_3O_4-PEG and soluble-Fe at 1 000 mg Fe L^{-1} and H_2O.

Figure 5. μ-XRF chemical maps for Fe in *P. vulgaris* seeds soaked in (a) nFe_3O_4-PEG and (b) soluble-Fe at 1 000 mg Fe L^{-1}.

Figure 6. Pictures of the hilum of *P. vulgaris* seeds soaked in (a) nFe_3O_4-PEG and (b) soluble-Fe at 1 000 mg Fe L^{-1} and its corresponding μ-XRF chemical maps for Fe.

Figure 7. X-ray tomograms of the hilum of a *P. vulgaris* seed treated with (a) Fe_3O_4-PEG nanoparticle and (b) soluble-Fe at 1 000 mg Fe L^{-1} dispersion for 20 min. The greenish spots highlighted by the red circles indicates the presence of Fe embedded in the organic tissue.
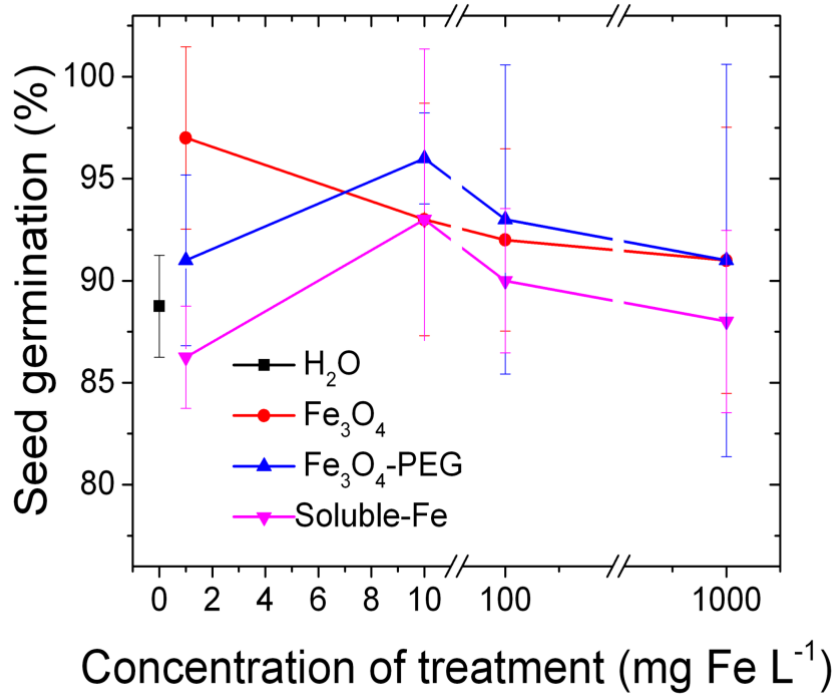
TABLES

Table 1. Zeta potential and hydrodynamic diameter of nFe_3O_4 and nFe_3O_4-PEG dispersions determined by Dynamic Light Scattering (DLS).

Magnetite type	Zeta-potential (mV)	Hydrodynamic Diameter (nm)		
		Peak 1	*Peak 2*	*Peak 3*
nFe_3O_4	-14 ± 7	71 ± 10 (12%)	310 ± 60 (88%)	--
nFe_3O_4-PEG	9 ± 6	170 ± 60 (54%)	480 ± 150 (41%)	$2\,700 \pm 160$ (5%)

FIGURES

Figure 1

Figure 2

a) H₂O

b) nFe₃O₄ (mg Fe L⁻¹)
1   10   100   1 000

c) nFe₃O₄-PEG (mg Fe L⁻¹)
1   10   100   1 000

d) Soluble-Fe (mg Fe L⁻¹)
1   10   100   1 000

Figure 3

a)

Radicle length (cm)

H₂O
Fe₃O₄
Fe₃O₄-PEG
Soluble-Fe

Concentration of treatment (mg Fe L⁻¹)

b)

Radicle fresh weight (g)

H₂O
Fe₃O₄
Fe₃O₄-PEG
Soluble-Fe

Concentration of treatment (mg Fe L⁻¹)
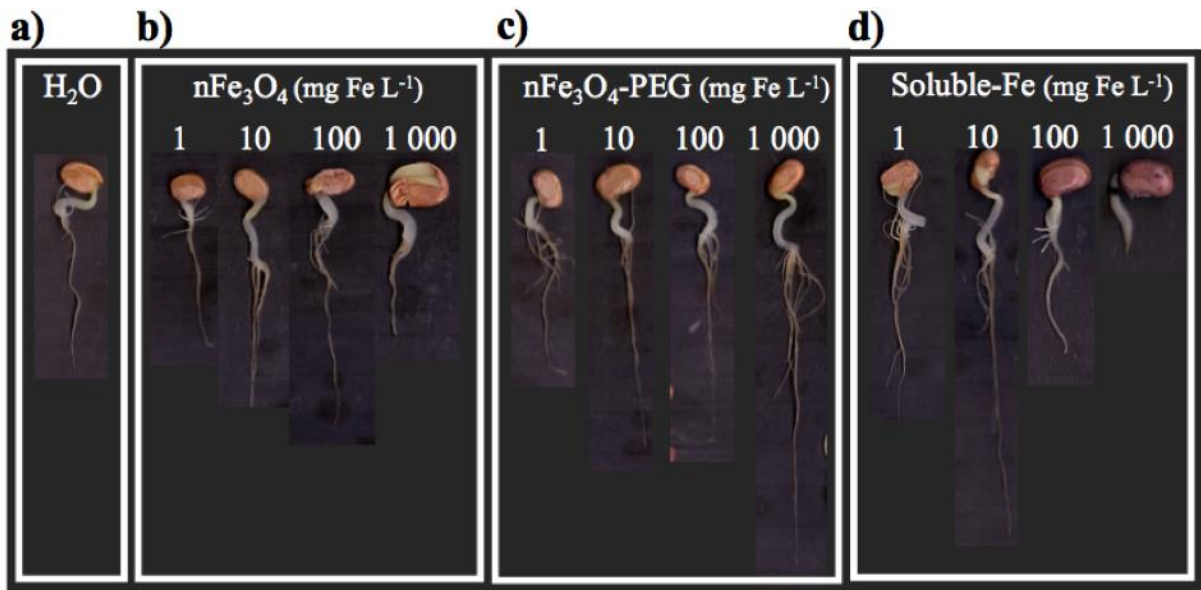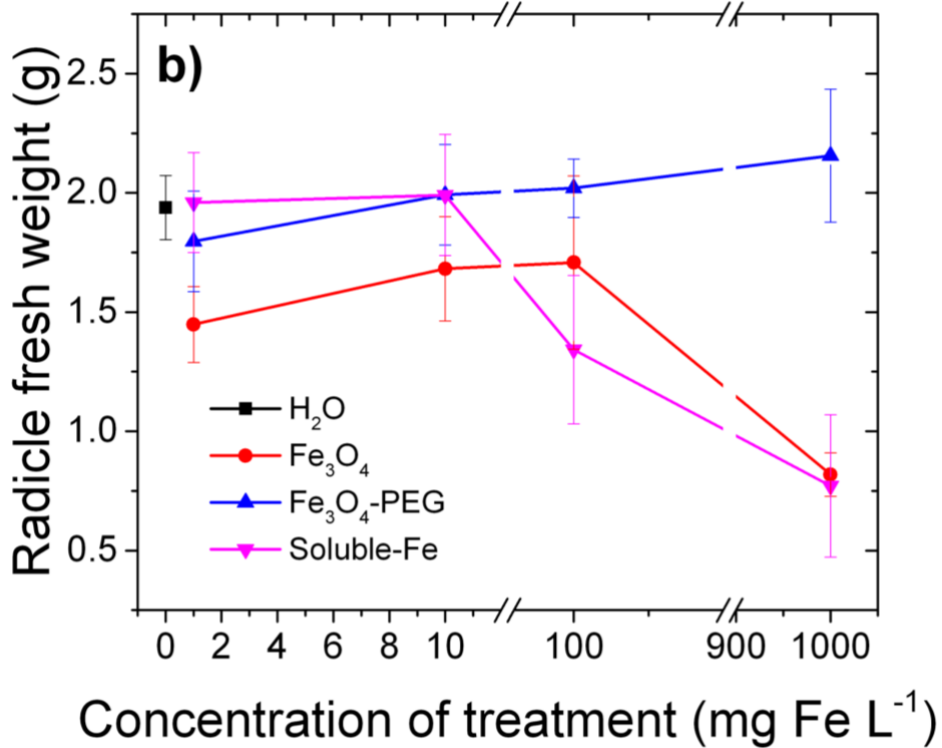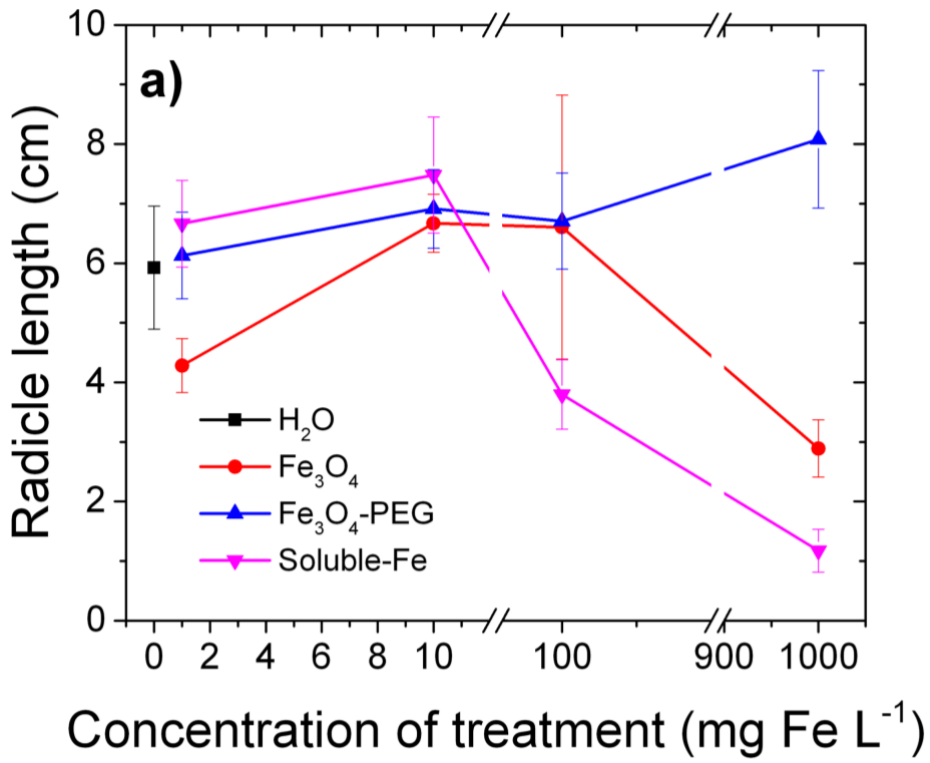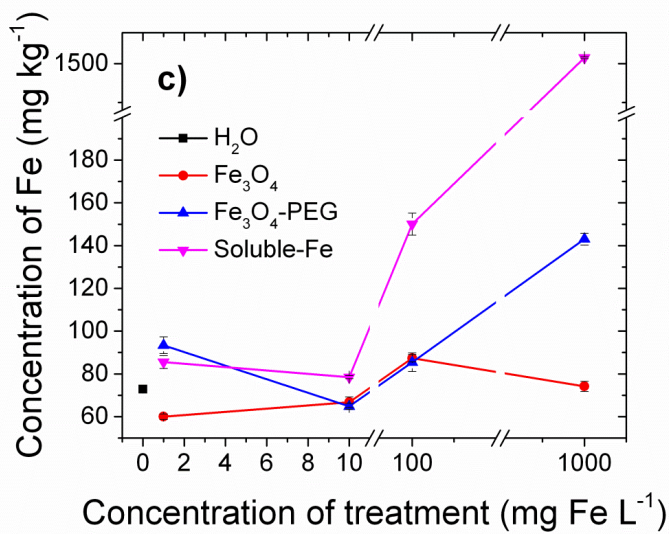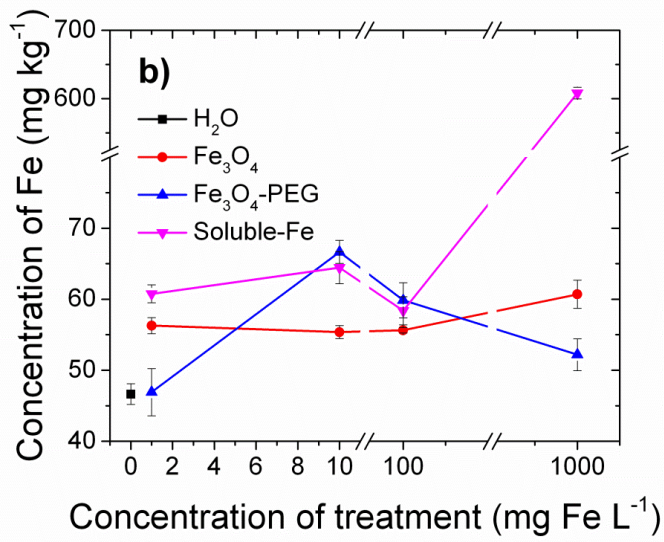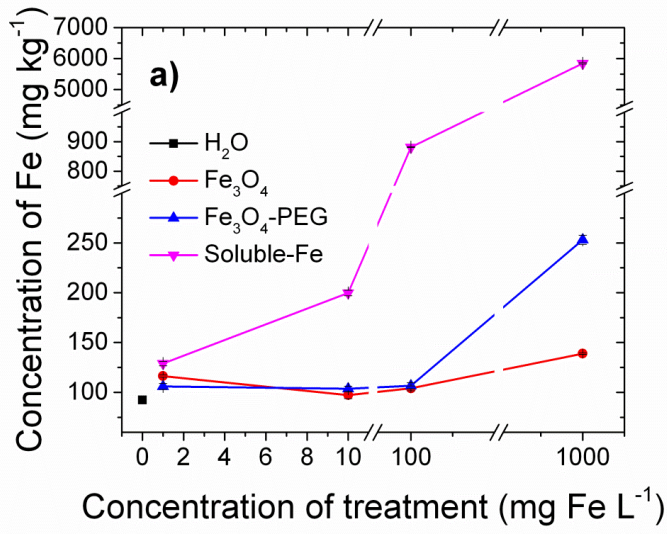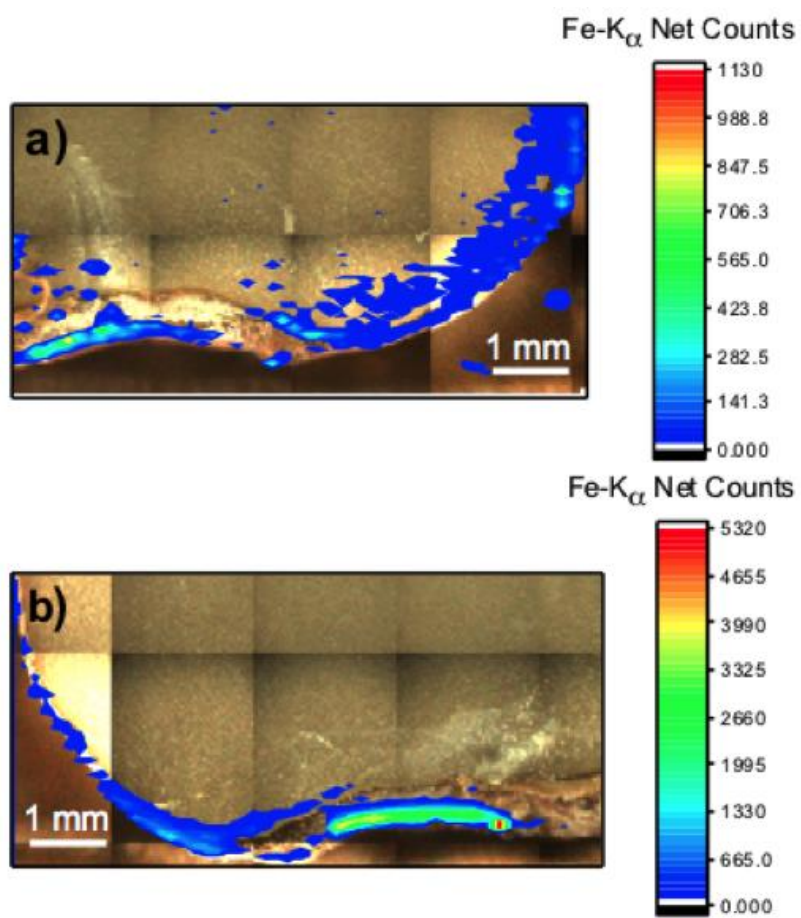
Figure 4

Figure 5

Figure 6
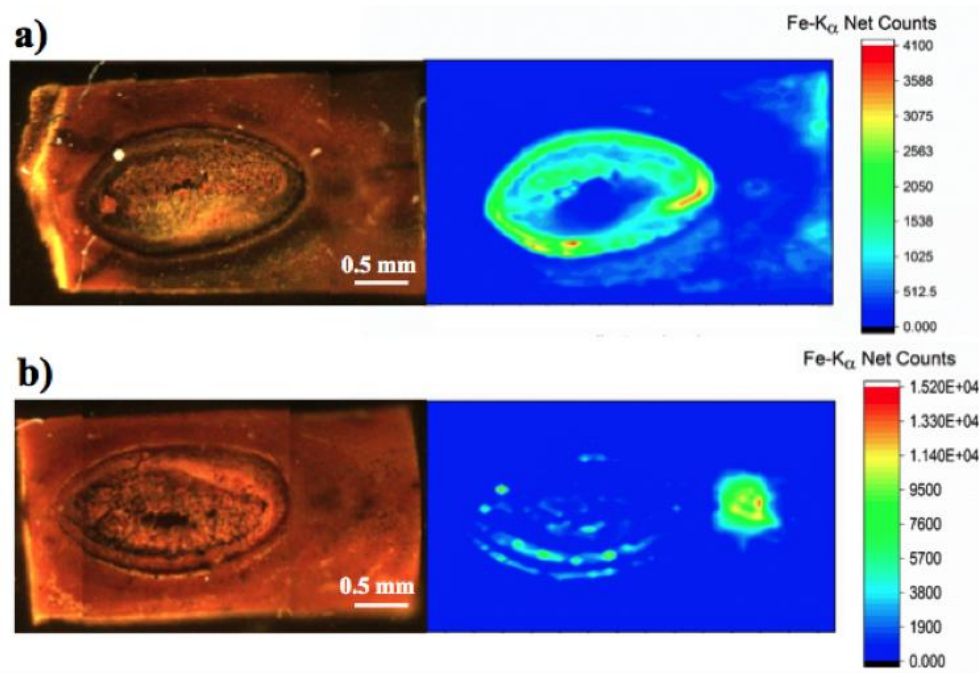
Figure 7
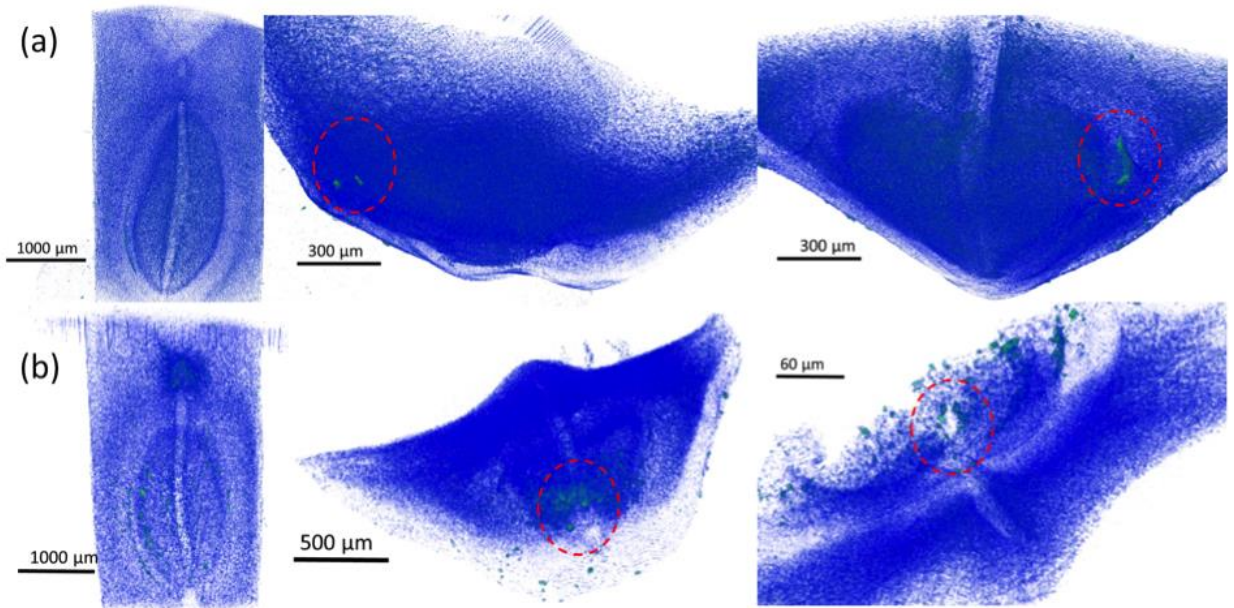
GRAPHIC FOR TABLE OF CONTENTS

DRAFT